Hindawi
Journal of Nanomaterials
Volume 2021, Article ID 6685355, 9 pages
https://doi.org/10.1155/2021/6685355

*Research Article*

# Controllable Architecture of Mesoporous Double-Nanoshell $SiO_2/TiO_2$ Hollow Tube Based on Layer by Layer Method

**Zhenzhong Chen,[1] Jia Li,[2] Zheng Zhang,[2] Jun-fa Liang,[3] Qizhi Luo,[2] and Xuncai Chen[2]**

[1]*School of Mechanical Engineering, Sungkyunkwan University, Suwon 16419, Republic of Korea*
[2]*School of Forensic Medicine, Southern Medical University, Guangzhou, Guangdong 510515, China*
[3]*Guangzhou Institute of Food Inspection, Guangzhou, Guangdong 511405, China*

Correspondence should be addressed to Qizhi Luo; luoqizhi12@126.com and Xuncai Chen; xche3815@smu.edu.cn

Received 16 December 2020; Revised 24 December 2020; Accepted 13 January 2021; Published 29 January 2021

Academic Editor: Wenjie Liu



Double-shell tubular on-dimensional structure can be fabricated through a layer by layer method, in which the core template was removed to create the tubular shape. In this paper, we report, for the first time, the double nanoshell $SiO_2/TiO_2$ hollow tubes prepared through a layer-by-layer deposition method involving the sol-gel process for the $SiO_2$ and $TiO_2$ generation. During TEOS and TEOT hydrolysis/condensation for the $SiO_2$ and $TiO_2$ shell layer formation, cetyltrimethylammonium bromide (CTAB) is adopted both as the structure-directing template and as the mesopore-channel template distributing around the shell. The obtained double-nanoshell hollow tubes illustrate a large surface area and high pore volume. Also, mesoporous double-nanoshell $SiO_2/TiO_2$ hollow tubes have the inner and outer shell thickness of about 80 nm and 120 nm, respectively. Plus, the shell thickness of $SiO_2$ and $TiO_2$ is controllable depending on the used concentration of TEOS and TEOT during their sol-gel process. Therefore, the technique for the preparation of $SiO_2/TiO_2$ mesoporous double-nanoshell hollow tubes could provide new insights into the construction of mesoporous double-shell and hollow structure for other multicomponent and hierarchical hybrid systems.

## 1. Introduction

Hollow-structured mesoporous materials with unique features of high surface area, high permeability, low density, confined inner cavity, and optical properties have been of great interest and received much research, which makes them a promising application in drug delivery systems [1–3], chemical and catalysts [4–10], biological sensors [11–17], and solar cells [18–20]. For example, the inner cavity of the hollow structure is very essential for drug delivery by offering a large volume transportation for DNA, drugs, and cosmetics [21, 22]. In addition, the inner- and outer-shell surface provides more active sites; when contacting with reactant molecules, the hollow-structured materials would display high sensor and catalytic activities [23–26]. Also, the hollow-structured materials enable to enhance the light-scattering effect through adjusting the refractive indices of the empty inner cavity and solid shell [19, 27]. Even with these advantages of hollow-structured material, the design of an optimized structure based on the hollow-structure to further enhance their performance for specific application fields remains a challenge.

To improve the advantages of the hollow structure, multishell hollow-structured materials have recently been considered to be a promising structure owning to their unique properties, such as large surface area, multiple components, and outstanding light-scattering effect [28–31]. The light scattering was enhanced through repeated reflection and scattering events between the inner and outer shells in the multishell structure. Furthermore, the multishell structure has a larger active surface area when comparing with a single shell one, which is because of the increasing surface area by the additional inner shells. As a result, the fabrication of multishell hollow-structured materials with enhanced performance in various applications has been widely studied. For example, a double-shell $LiMn_2O_4$ hollow sphere was

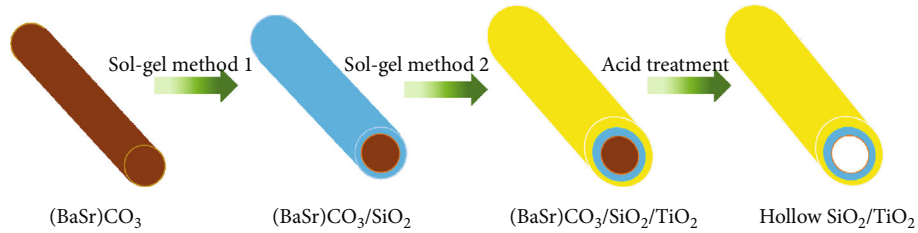


Scheme 1: Schematic representation of the synthesis of mesoporous double-nanoshell $SiO_2/TiO_2$ hollow tube.

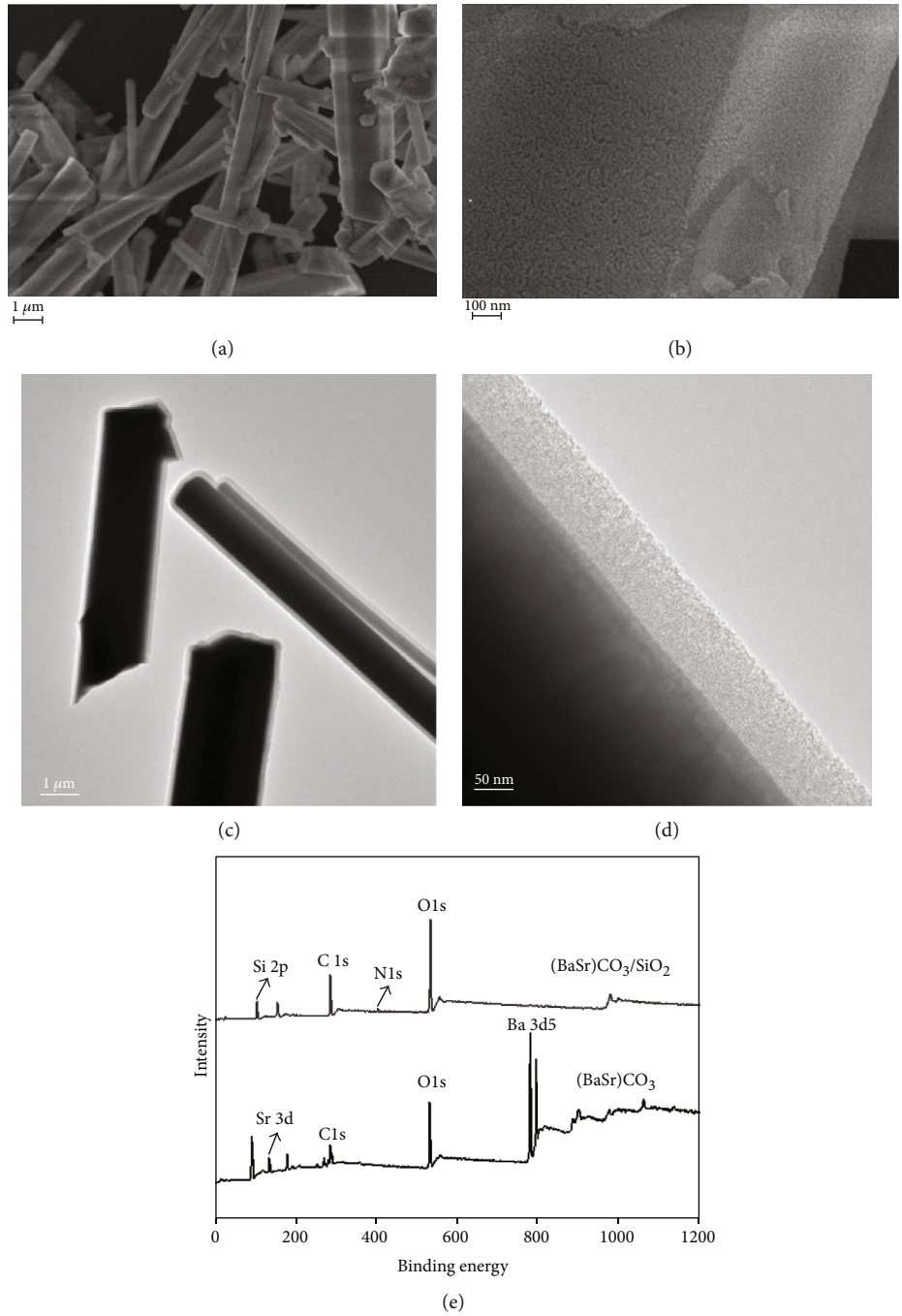


Figure 1: (a) FE-SEM images of $(BaSr)CO_3/SiO_2$ core@shell rods and (b) high resolution of $(BaSr)CO_3/SiO_2$ core@shell rod surface. (c) FE-TEM image of $(BaSr)CO_3/SiO_2$ core@shell rods, and (d) FE-TEM image of the interface of $(BaSr)CO_3/SiO_2$ core@shell rod. (e) XPS spectra of $(BaSr)CO_3$ and $(BaSr)CO_3/SiO_2$ core@shell rods.

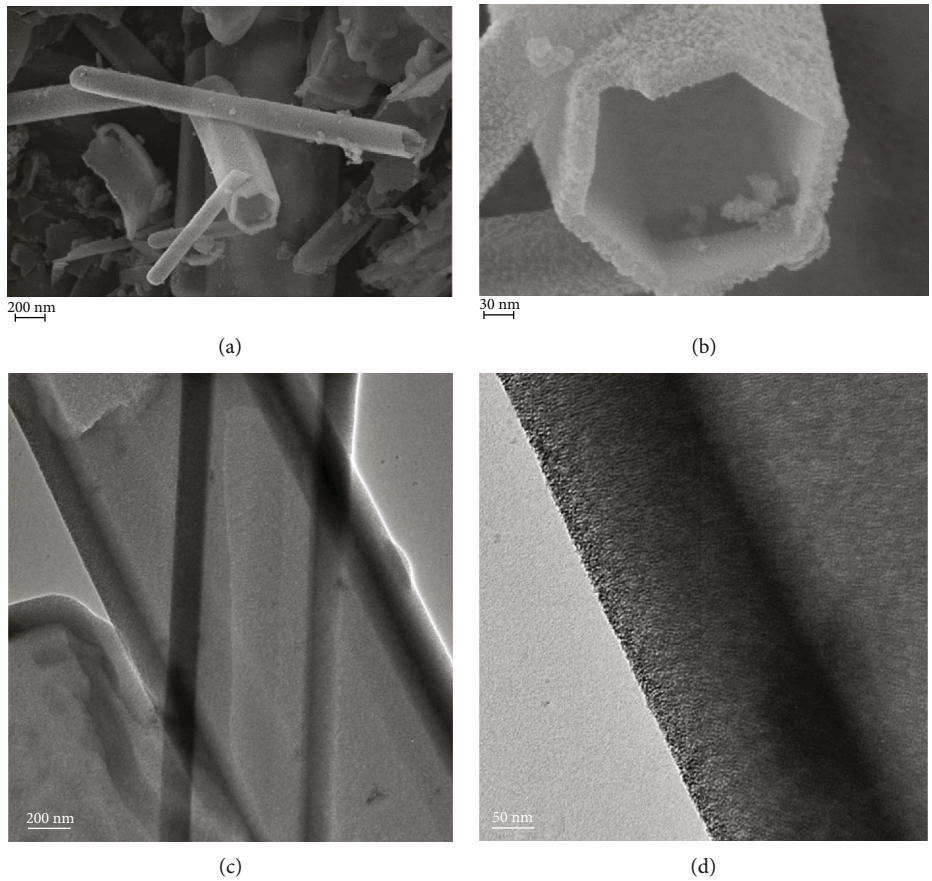


Figure 2: (a) FE-SEM images of $SiO_2$ hollow tube and (b) high resolution of hollow tube. (c) FE-TEM image of the hollow tube, and (d) FE-TEM image of the interface of hollow tube.

fabricated by using a hydrothermal synthesis method to optimize the performance of lithium-ion batteries [32]. With the double-shell configuration, the battery showed improved performance, which was ascribed to the larger contact area between the electrolyte and electrode generated by the gap and hollow interior between the shells. In addition, multishell hollow spheres of microscale ZnO were prepared via the hydrothermal method by Zhang et al., which presented extraordinary sensitivity for the detection of toluene [33]. Furthermore, the double-shell $TiO_2$ hollow spheres were prepared via the hydrothermal method by Wu et al., exhibiting a reinforced light-scattering ability in the application of dye-sensitized solar cell (DSSC) [34]. However, hydrothermal reactions using an autoclave were mainly adopted to fabricate multishell hollow structures in the previous approach, which easily resulted in the size uncontrollable and particle aggregation inevitable because of high reaction temperature and high pressure involved. Therefore, methods for synthesizing particles with multishell hollow structure at the nanoscale were in growing demand.

Recently, layer-by-layer (LBL) assembly has already been proved to be a simple, convenient, and controllable method for the design and fabrication of core-shell/core-double-shell particles with tailored chemical composition and controllable architecture on varied substrate surfaces [35–41]. Xing et al. synthesized stable colloidal gold-collagen core-shell nanoconjugates with improved mechanical properties by using the LBL assembly method [42]. In addition, Liao and coworkers the unique $TiO_2$-C/$MnO_2$ core-double-shell nanowires using as anode materials for lithium-ion batteries was prepared by layer-by-layer deposition approach [43]. It is not hard to imagine that the core-double-shell particle could be converted to a double-shell hollow particle, when its core was removed. Thus, the layer-by-layer assembly method was supposed to be an applicative approach to fabricate multishell hollow particles.

Herein, we report the synthesis of $SiO_2/TiO_2$ mesoporous double-shell hollow tubes from (BaSr)$CO_3/SiO_2/TiO_2$ core-double-nanoshell rods based on the layer-by-layer method. It should be mentioned that the hybrid $SiO_2/TiO_2$ particles have been proved to be a versatile material for various application, such as self-cleaning and antireflective coatings, electrorheological fluids, and photocatalysts [44–54]. In this work, the $SiO_2/TiO_2$ double-shell hollow tubes was prepared via selectively removing the core material from the (BaSr)$CO_3/SiO_2/TiO_2$ core-double-shell rods. In addition, the thickness of $SiO_2$ and $TiO_2$ shell can be easily controlled by regulating the concentration of tetraethyl orthosilicate (TEOS) and tetraethyl titanate (TEOT). Lastly, the formation mechanism for the double-shell $SiO_2/TiO_2$ hollow tubes was also studied.

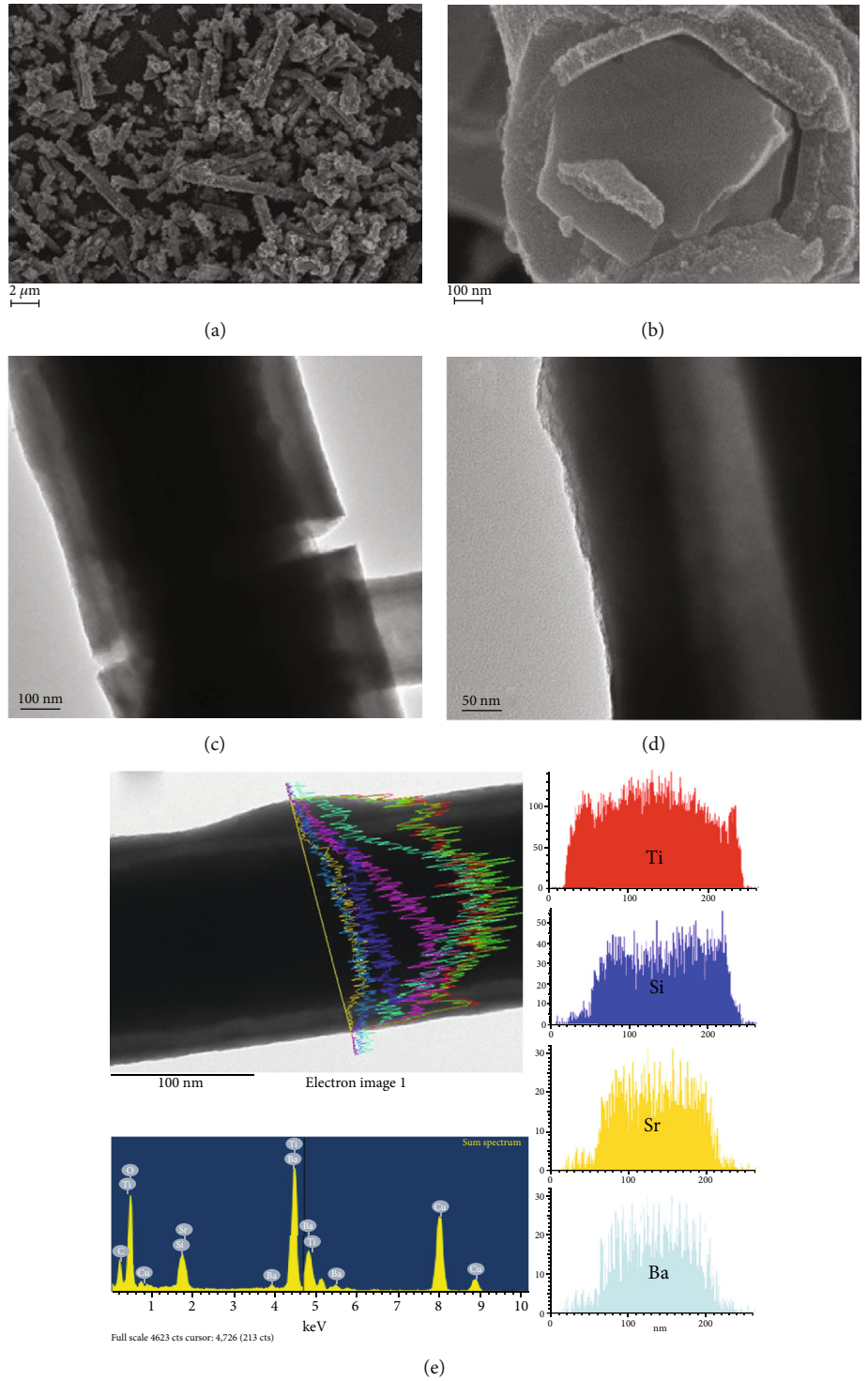


FIGURE 3: (a) FE-SEM images of $(BaSr)CO_3/SiO_2/TiO_2$ core@ double-shell rods and (b) high resolution of cross-section view of $(BaSr)CO_3/SiO_2/TiO_2$ core@ double-shell rods. (c) FE-TEM image of $(BaSr)CO_3/SiO_2/TiO_2$ core@ double-shell rods, and (d) FE-TEM image of interface of $(BaSr)CO_3/SiO_2/TiO_2$ core@ double-shell rods. (e) EDS line scanning analysis of Ba, Sr, Si, and Ti in $(BaSr)CO_3/SiO_2/TiO_2$ core@ double-shell rod.

## 2. Experimental Section

*2.1. Synthesis of $SiO_2$ Hollow Tubes.* Firstly, $(BaSr)CO_3$ was prepared by our previously reported coprecipitation method; the details can be seen in literatures [52–54]. Subsequently, 1.0 g $(BaSr)CO_3$ white powders were dispersed in 40 ml of water and then added 2 ml of aqueous ammonia solution (25~28 wt%), 60 ml of ethanol, and 1.0 g of CTAB. Then,

100 ml of TEOS solution ($6 \times 10^{-3}$ ml-TEOS/ml-$H_2O$) was slowly fed into the above suspension at a flow rate of 0.2 ml/min under rigorous agitation at 30°C. After complete feeding, the product suspension was continuously stirred for 2 h. The final product suspension was filtered out using a filter paper and washed with water and ethanol several times to attain the (BaSr)$CO_3$/$SiO_2$ core@shell rods. Next, the core@shell rods were added into the 10% HCl solution to generate the $SiO_2$ hollow tubes.

*2.2. Synthesis of (BaSr)$CO_3$/$SiO_2$/$TiO_2$ Core@ Double-Nanoshell Rods and $SiO_2$/$TiO_2$ Double-Nanoshell Hollow Tubes.* The above (BaSr)$CO_3$/$SiO_2$ core@shell rods were dispersed in 100 ml of ethanol and then mixed 0.25 g of CTAB and 0.2 ml of pure TEOT reagent, followed by slow feeding 2 ml of $H_2O$ into the above (BaSr)$CO_3$/$SiO_2$ core@shell rod suspension with a pump at a flow rate of 0.1 ml/min under rigorous agitation at 30°C. After complete feeding, the product suspension was continuously stirred for 20 h. The final product suspension was filtered out using a filter paper and washed several times with water and ethanol. Next, the attained (BaSr)$CO_3$/$SiO_2$/$TiO_2$ core@ double-nanoshell rods were calcinated at 350°C to remove CTAB and then was added into the 1 M HCl to dissolve (BaSr)CO3 core materials. Finally, the resulting sample was filtered out using a filter paper and washed several times with water and ethanol.

*2.3. Characterizations.* The size and shape of (BaSr)$CO_3$/$SiO_2$ core@shell rods, $SiO_2$ hollow tubes, (BaSr)$CO_3$/$SiO_2$/$TiO_2$ core@ double-shell rods, and $SiO_2$/$TiO_2$ double-shell hollow tubes were measured by using an FE-SEM (LEO SUPRA 55 microscope, Carl Zeiss, Germany) and FE-TEM (using a JEM-2100F microscope operated at 200 kV). Their structure was also analyzed by powder X-ray diffraction (M18XHF-SRA, Mac Science, Japan) with Cu K$\alpha$ radiation ($\lambda = 1.54056$ Å). The X-ray photoelectron spectroscopy (XPS) spectra were observed using a Quantum 2000 XPS system (Physical Electronics, Inc.). The atomic composition of the rods was analyzed by using EDS element mapping (Oxford INCA Resolution 30 $mm^2$ 136 eV at Mn K$\alpha$ 5 B to 92 U). Finally, the surface areas were calculated using the Brunauer-Emmett-Teller (BET) method, and the pore sizes were calculated using the Barrett-Joyner-Hatenda (BJH) model (BELSORP-max(MP), Japan).

## 3. Results and Discussion

*3.1. Synthesis of (BaSr)$CO_3$/$SiO_2$ Core@Shell Rods and $SiO_2$ Hollow Tubes.* First, the core@shell structure of (BaSr)$CO_3$/$SiO_2$ was prepared based on the sol-gel method, as shown in Scheme 1. The structure and composition of (BaSr)$CO_3$ core have been discussed in the published paper by current authors [54, 55]. As shown in Figures 1(b) and 1(d), the rod-shaped (BaSr)$CO_3$/$SiO_2$ core@shell with a uniform thickness of around 80 nm was attained. Particularly, from XPS spectra (Figure 1(e)), the peaks for Sr 3d and Ba 3d5 in (BaSr)$CO_3$/$SiO_2$ core-shell rods disappeared, while new peaks appeared for Si 2p assigned to $SiO_2$. Therefore, this result

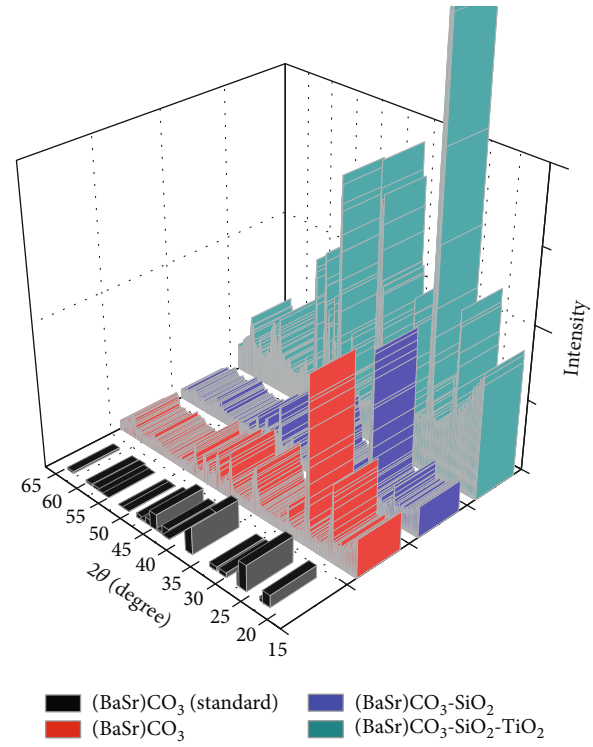


FIGURE 4: XRD patterns of (BaSr)$CO_3$, (BaSr)$CO_3$/$SiO_2$ core@shell rods, (BaSr)$CO_3$/$SiO_2$/$TiO_2$ core@ double-shell rods, and the (BaSr)$CO_3$ reference: JCPDS no. 47-0223.

also indicated that the (BaSr)$CO_3$ core was fully covered with $SiO_2$ shell. In addition, the thickness of $SiO_2$ shell layer could be controlled by tuning the concentration of TEOS, as shown in Supplementary Figure 1. As a result, the thickness of $SiO_2$ shell layer increased from 40 nm to 180 nm when increasing the TEOS concentration from 0.2% to 0.8%. After that, the (BaSr)$CO_3$ core was removed by dissolving in the acid solution. Then, the $SiO_2$ hexagonal tubes with a rough surface were produced as shown in Figure 2. In this tubular structure of $SiO_2$, the outer diameters were around 600 nm~800 nm and the wall thickness was 80 nm. The CTAB was used as the template for the structure-directing polymerization during the $SiO_2$ and $TiO_2$ formation. Thus, before dissolving the (BaSr)$CO_3$ into an acid solution, the CTAB was calcinated at 350°C to remove the CTAB; the mesopores were created on the $SiO_2$ shell, which was confirmed by the high-resolution TEM analysis (Figure 2(d)). The TEM images showed perpendicularly directed pore channels in the $SiO_2$ shell.

*3.2. Synthesis of (BaSr)$CO_3$/$SiO_2$/$TiO_2$ Core@ Double-Shell Rods and $SiO_2$/$TiO_2$ Double-Nanoshell Hollow Tubes.* According to the layer-by-layer method, the $TiO_2$ outer layer was successfully coated on the surface of the (BaSr)$CO_3$/$SiO_2$ core@shell rods by a sol-gel method to form the (BaSr)$CO_3$/$SiO_2$/$TiO_2$ core@ double-shell rods. From the cross-section view (Figure 3(b)), the first boundary between the core and $SiO_2$ inner layer, and the second boundary between $SiO_2$ inner layer and $TiO_2$ outer layer were clearly presented. In

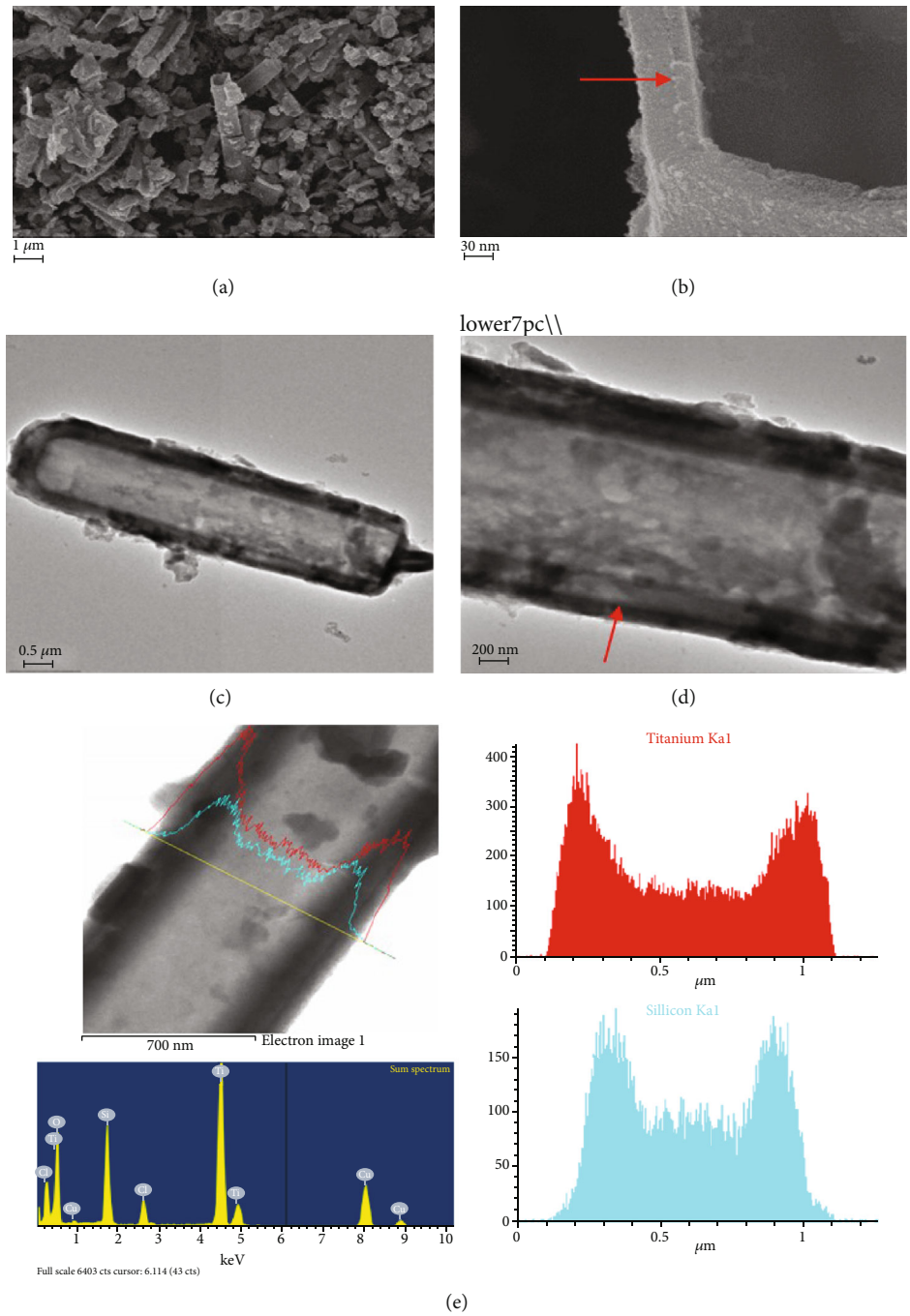


FIGURE 5: (a) FE-SEM images of $SiO_2/TiO_2$ double-nanoshell hollow tubes and (b) high resolution of $SiO_2/TiO_2$ double-nanoshell hollow tube edge. (c) FE-TEM image of $SiO_2/TiO_2$ double-nanoshell hollow tubes, and (d) FE-TEM image of the interface of $SiO_2/TiO_2$ double-nanoshell hollow tubes. (e) EDS line scanning analysis of Si and Ti in $SiO_2/TiO_2$ double-nanoshell hollow tubes.

particular, the inner shell with a thickness of around 80 nm uniformly wrapped the core, and the 120 nm thick outer shell homogenously wrapped the inner shell. In addition, the TEM images confirmed the core@double-nanoshell structure of $(BaSr)CO_3/SiO_2/TiO_2$ (Figures 3(c) and 3(d)). The EDS line detection showed that the metal ions were only found in the core region, and the Si covered the diameter of the core and inner shell, whereas Ti overridden the total diameter of the $(BaSr)CO_3/SiO_2/TiO_2$ core@double-nanoshell rods, strongly suggesting a core@double-nanoshell structure of $(BaSr)CO_3/SiO_2/TiO_2$. In addition, the XRD pattern (Figure 4) shows there is no difference among the $(BaSr)CO_3$ core, $(BaSr)CO_3/SiO_2$, and $(BaSr)CO_3/SiO_2/TiO_2$, that is because of the amorphous form of the $SiO_2$ and $TiO_2$. Similar to the silica formation, the thickness of the $TiO_2$ shell also could be adjusted by controlling the concentration of TEOT. The thickness of $TiO_2$ varies from 20 nm to 160 nm, when increasing the concentration of TEOT from 0.05 ml to

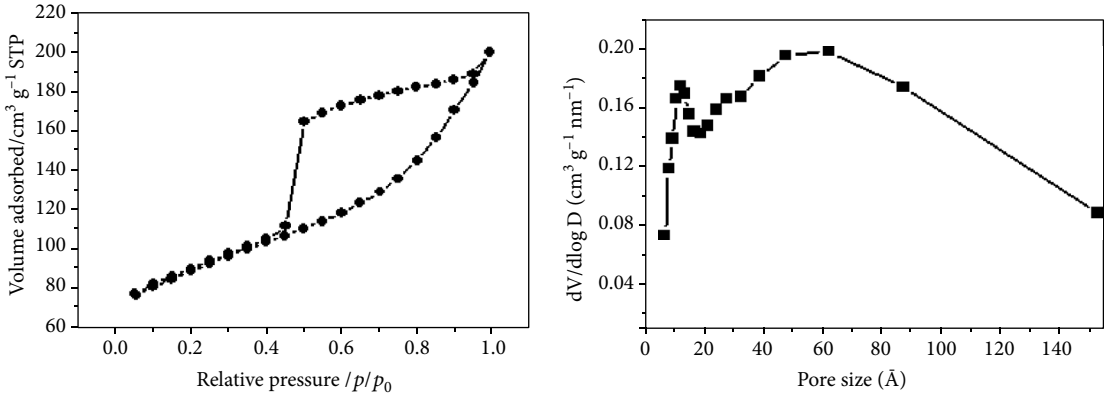


FIGURE 6: Structural characterization of $SiO_2/TiO_2$ double-nanoshell hollow tubes: (a) nitrogen adsorption-desorption isotherms and (b) pore size distribution calculated from the adsorption branch of isotherms.

0.25 ml, as shown in Supplementary Figure 2. Next, the $SiO_2/TiO_2$ double-shell hollow tubes were prepared by removing the core template. The boundary between the double-shell was obviously seen in the hollow tube structure (Figures 5(b) and 5(d)). Besides, the TEM analysis also confirms the tubular structure and presented the double shell. The EDS line presented a valley-like intensity profile of Si concentrating on the inner shell and Ti centralized on the outer shell, which further proved the formation of $SiO_2/TiO_2$ double-shell hollow tubes. Similarly, during the formation of $TiO_2$, the CTAB was continually employed as the template for the structure-directing polymerization of $TiO_2$ uniform formation, which suggests that the pores would be created in the double-shell of $SiO_2/TiO_2$ when removing the CTAB by calcinating at 350°C. Then, nitrogen physisorption characterization was used to confirm the porosity of the $SiO_2/TiO_2$ double-shell hollow tubes, which illustrated that the tubes were mesoporous based on the nitrogen adsorption-desorption isotherms (Figure 6(a)), as identified by the increase of the adsorption amount in the relative pressure ($P/P_0$) range of 0.2-0.4. In addition, the pore size distribution curve calculated from the adsorption branch of the isotherms (Figure 6(b)) was around 1 nm to 14 nm, and the surface area of the $SiO_2$ tubes was calculated to be 304 $m^2g^{-1}$, demonstrating a highly mesoporous double-nanoshell and high surface area of the tube.

The $SiO_2/TiO_2$ double-nanoshell hollow tubes not only could be applied as light scattering material for highly efficient dye-sensitized solar cells but also enable to be used as camptothecin (CPT) delivery agents for cancer treatment. Details of their potential application will be reported in due course.

## 4. Conclusion

In conclusion, the $SiO_2$ hollow tubes and $SiO_2/TiO_2$ double-nanoshell hollow tubes were successfully prepared based on a layer-by-layer method. The as-prepared $SiO_2/TiO_2$ double-nanoshelll layer is highly porous and has large surface area, allowing direct interaction between the inner surface of the tube and its surrounding environment. In addition, the layer thickness both of $SiO_2$ and $TiO_2$ is adjustable by controlling their used concentration. Therefore, the technique for the preparation of $SiO_2/TiO_2$ double-nanoshell hollow tubes can clearly be extended to other mesoporous double-shell architectures and hollow structure of other dimensions and also could be used as a platform for multicomponent, hierarchical hybrid systems. Finally, the proposed method represents a relevant and directed approach to the design of new and novel hollow particles specialized for various applications at the discretion of the end-users.

## Data Availability

All data generated or analyzed during this study are included within the article.

## Conflicts of Interest

The authors declare that they have no conflicts of interest.

## Acknowledgments

This work was supported by the Southern Medical University (grant no: G620522046).

## Supplementary Materials

Results: influence of TEOS and TEOT concentration on double shell thickness. *(Supplementary Materials)*

## References

[1] F. P. Dong, I. Firkowska-Boden, M. M. L. Arras, and K. D. Jandt, "Responsive copolymer–graphene oxide hybrid microspheres with enhanced drug release properties," *RSC Advances*, vol. 7, no. 7, pp. 3720–3726, 2017.

[2] Y. H. Li, N. Li, W. Pan, Z. Z. Yu, L. M. Yang, and B. Tang, "Hollow mesoporous silica nanoparticles with tunable

structures for controlled drug delivery," *ACS Applied Materials & Interfaces*, vol. 9, no. 3, pp. 2123–2129, 2017.

[3] Y. J. Zhu, X. X. Guo, and T. K. Sham, "Calcium silicate-based drug delivery systems," *Expert Opinion on Drug Delivery*, vol. 14, no. 2, pp. 215–228, 2017.

[4] J. F. Chang, Q. Lv, G. Q. Li, J. J. Ge, C. P. Liu, and W. Xing, "Core-shell structured $Ni_{12}P_5/Ni_3(PO_4)_2$ hollow spheres as difunctional and efficient electrocatalysts for overall water electrolysis," *Applied Catalysis B: Environmental*, vol. 204, pp. 486–496, 2017.

[5] F. A. La Porta, A. E. Nogueira, L. Gracia et al., "An experimental and theoretical investigation on the optical and photocatalytic properties of ZnS nanoparticles," *Journal of Physics and Chemistry of Solids*, vol. 103, pp. 179–189, 2017.

[6] C. Liu, J. Wang, J. S. Li et al., "Fe/N decorated mulberry-like hollow mesoporous carbon fibers as efficient electrocatalysts for oxygen reduction reaction," *Carbon*, vol. 114, pp. 706–716, 2017.

[7] Y. Peng, K. K. Wang, T. Liu, J. Xu, and B. Xu, "Synthesis of one-dimensional $Bi_2O_3$-$Bi_2O_{2.33}$ heterojunctions with high interface quality for enhanced visible light photocatalysis in degradation of high-concentration phenol and MO dyes," *Applied Catalysis B: Environmental*, vol. 203, pp. 946–954, 2017.

[8] T. Tesfu-Zeru, M. Sakthivel, and J. F. Drillet, "Investigation of mesoporous carbon hollow spheres as catalyst support in DMFC cathode," *Applied Catalysis B: Environmental*, vol. 204, pp. 173–184, 2017.

[9] J. S. Zhang, T. J. Yao, C. C. Guan et al., "One-step preparation of magnetic recyclable quinary graphene hydrogels with high catalytic activity," *Journal of Colloid and Interface Science*, vol. 491, pp. 72–79, 2017.

[10] T. S. Zhou, Y. Zhou, R. G. Ma et al., "Nitrogen-doped hollow mesoporous carbon spheres as a highly active and stable metal-free electrocatalyst for oxygen reduction," *Carbon*, vol. 114, pp. 177–186, 2017.

[11] J. J. Jiang, K. Zhang, X. D. Chen et al., "Porous Ce-doped ZnO hollow sphere with enhanced photodegradation activity for artificial waste water," *Journal of Alloys and Compounds*, vol. 699, pp. 907–913, 2017.

[12] L. Qiao, Y. F. Bing, Y. Z. Wang, S. S. Yu, Z. Z. Liang, and Y. Zeng, "Enhanced toluene sensing performances of Pd-loaded $SnO_2$ cubic nanocages with porous nanoparticle-assembled shells," *Sensors & Actuators, B: Chemical*, vol. 241, pp. 1121–1129, 2017.

[13] Q. Y. Yang, Y. L. Wang, J. Liu et al., "Enhanced sensing response towards $NO_2$ based on ordered mesoporous Zr-doped $In_2O_3$ with low operating temperature," *Sensors & Actuators, B: Chemical*, vol. 241, pp. 806–813, 2017.

[14] T. Y. Yang, H. Yu, B. X. Xiao, Z. F. Li, and M. Z. Zhang, "Enhanced 1-butylamine gas sensing characteristics of flower-like $V_2O_5$ hierarchical architectures," *Journal of Alloys and Compounds*, vol. 699, pp. 921–927, 2017.

[15] S. Zhang, P. Song, J. Li, J. Zhang, Z. X. Yang, and Q. Wang, "Facile approach to prepare hierarchical Au-loaded $In_2O_3$ porous nanocubes and their enhanced sensing performance towards formaldehyde," *Sensors & Actuators, B: Chemical*, vol. 241, pp. 1130–1138, 2017.

[16] S. Zhang, P. Song, J. Zhang et al., "Highly sensitive detection of acetone using mesoporous $In_2O_3$ nanospheres decorated with Au nanoparticles," *Sensors & Actuators, B: Chemical*, vol. 242, pp. 983–993, 2017.

[17] T. T. Zhou, T. Zhang, R. Zhang et al., "Highly sensitive sensing platform based on $ZnSnO_3$ hollow cubes for detection of ethanol," *Applied Surface Science*, vol. 400, pp. 262–268, 2017.

[18] R. Ahmad, J. K. Kim, J. H. Kim, and J. Kim, "Well-organized, mesoporous nanocrystalline TiO2 on alumina membranes with hierarchical architecture: antifouling and photocatalytic activities," *Catalysis Today*, vol. 282, pp. 2–12, 2017.

[19] R. K. Chava, W. M. Lee, S. Y. Oh, K. U. Jeong, and Y. T. Yu, "Improvement in light harvesting and device performance of dye sensitized solar cells using electrophoretic deposited hollow $TiO_2$ NPs scattering layer," *Solar Energy Materials & Solar Cells*, vol. 161, pp. 255–262, 2017.

[20] J. Li, H. Z. Cui, X. J. Song, N. Wei, and J. Tian, "The high surface energy of NiO {110} facets incorporated into $TiO_2$ hollow microspheres by etching Ti plate for enhanced photocatalytic and photoelectrochemical activity," *Applied Surface Science*, vol. 396, pp. 1539–1545, 2017.

[21] J. P. Shi, M. Sun, X. Sun, and H. W. Zhang, "Near-infrared persistent luminescence hollow mesoporous nanospheres for drug delivery and in vivo renewable imaging," *Journal of Materials Chemistry B*, vol. 4, no. 48, pp. 7845–7851, 2016.

[22] H. S. Varol, O. Alvarez-Berrmudez, P. Dolcet et al., "Crystallization at nanodroplet interfaces in emulsion systems: a soft-template strategy for preparing porous and hollow nanoparticles," *Langmuir*, vol. 32, no. 49, pp. 13116–13123, 2016.

[23] X. Y. Li, H. Liu, S. Liu et al., "Effect of Pt-Pd hybrid nanoparticle on CdS's activity for water splitting under visible light," *International Journal of Hydrogen Energy*, vol. 41, no. 48, pp. 23015–23021, 2016.

[24] M. Tian, X. L. Cui, C. X. Dong, and Z. P. Dong, "Palladium nanoparticles dispersed on the hollow aluminosilicate [email protected] $\gamma$-AlOOH as an excellent catalyst for the hydrogenation of nitroarenes under ambient conditions," *Applied Surface Science*, vol. 390, pp. 100–106, 2016.

[25] Q. Wang, R. G. Zhang, L. T. Jia, B. Hou, D. B. Li, and B. J. Wang, "Insight into the effect of surface coverage and structure over different Co surfaces on the behaviors of $H_2$ adsorption and activation," *International Journal of Hydrogen Energy*, vol. 41, no. 48, pp. 23022–23032, 2016.

[26] Q. M. Wang, S. G. Chen, F. Shi et al., "Structural Evolution of Solid Pt Nanoparticles to a Hollow PtFe Alloy with a Pt-Skin Surface via Space-Confined Pyrolysis and the Nanoscale Kirkendall Effect," *Advanced Materials*, vol. 28, pp. 10673–10678, 2016.

[27] S. Q. Xu, X. J. Xu, M. Xu, T. R. O'Leary, and L. N. Zhang, "Heat-induced conformation transition of the comb-branched $\beta$-glucan in dimethyl sulfoxide/water mixture," *Carbohydrate Polymer*, vol. 157, pp. 1404–1412, 2017.

[28] Z. G. An and J. J. Zhang, "Glass–NiP–CoFeP triplex-shell particles with hollow cores and tunable magnetic properties," *ACS Applied Materials & Interfaces*, vol. 5, no. 3, pp. 989–996, 2013.

[29] M. Y. Gao, Y. H. Zhao, S. H. Zeng, and H. Q. Su, "Multishell hollow CeO2/CuO microbox catalysts for preferential CO oxidation in H2-rich stream," *Catalysis Communications*, vol. 72, pp. 105–110, 2015.

[30] S. Hong, J. A. I. Acapulco, H. Y. Jang, and S. Park, "Au nanodisk-core multishell nanoparticles: synthetic method for controlling number of shells and intershell distance," *Chemistry of Materials*, vol. 26, no. 12, pp. 3618–3623, 2014.

[31] X. C. Li, L. Wang, J. H. Shi, N. X. Du, and G. H. He, "Multi-shelled nickel–cobalt oxide hollow microspheres with

optimized compositions and shell porosity for high-performance pseudocapacitors," *ACS Applied Materials & Interfaces*, vol. 8, no. 27, pp. 17276–17283, 2016.

[32] S. Q. Liang, J. Yi, and A. Q. Pan, "Synthesis of Double-Shelled LiMn2O4 Hollow Microspheres with Enhanced Electrochemical Performance for Lithium Ion Batteries," *International Journal of Electrochemical Science*, vol. 8, pp. 6535–6543, 2013.

[33] L. L. Wang, Z. Lou, T. Fei, and T. Zhang, "Zinc oxide core–shell hollow microspheres with multi-shelled architecture for gas sensor applications," *Journal of Materials Chemistry*, vol. 21, no. 48, pp. 19331–19336, 2011.

[34] X. Wu, G. Q. Lu, and L. Z. Wang, "Shell-in-shell TiO2 hollow spheres synthesized by one-pot hydrothermal method for dye-sensitized solar cell application," *Energy & Environmental Science*, vol. 4, no. 9, pp. 3565–3572, 2011.

[35] H. N. Cao, J. He, L. Deng, and X. Q. Gao, "Fabrication of cyclodextrin-functionalized superparamagnetic $Fe_3O_4$/amino-silane core-shell nanoparticles via layer-by-layer method," *Applied Surface Science*, vol. 255, no. 18, pp. 7974–7980, 2009.

[36] J. Y. Chen, D. M. Chao, X. F. Lu, and W. J. Zhang, "Preparation of PS-Cores/Au nanoparticles and polyaniline-shells submicrospheres via layer-by-layer method," *Solid State Phenomen*, vol. 121-123, pp. 263–266, 2007.

[37] Y. P. Chen, Y. M. Xu, D. G. Cheng et al., "Synthesis of CuO–ZnO–Al2O3 @ SAPO-34 core@shell structured catalyst by intermediate layer method," *Pure and Applied Chemistry*, vol. 86, no. 5, pp. 775–783, 2014.

[38] B. Hwang, S. H. Jang, H. H. Ahn, J. Yoon, S. Y. Kim, and Y. K. Kwon, "Preparation of magnetite core-titania shell and hollow titania nanoparticles via layer-by-layer (LbL) assembly method," *Macromolecular Research*, vol. 22, no. 2, pp. 223–226, 2014.

[39] H. Y. Liu, Y. J. Song, S. S. Li et al., "Synthesis of core/shell structured Pd3Au@Pt/C with enhanced electrocatalytic activity by regioselective atomic layer deposition combined with a wet chemical method," *RSC Advances*, vol. 6, no. 71, pp. 66712–66720, 2016.

[40] F. P. Ramanery, A. A. P. Mansur, and H. S. Mansur, "Synthesis and characterization of water-dispersed CdSe/CdS core-shell quantum dots prepared via layer-by-layer method capped with carboxylic-functionalized poly(vinyl alcohol)," *Materials Research - Ibero-American Journal*, vol. 17, suppl 1, pp. 133–140, 2014.

[41] X. M. Wang, J. D. Song, and H. L. Chen, "Preparation of ZnO@void@SiO2Rattle Type Core–Shell Nanoparticles via Layer-by-Layer Method," *Nano*, vol. 11, no. 9, article 1650103, 2016.

[42] R. R. Xing, T. F. Jiao, K. Ma, G. H. Ma, H. Mohwald, and X. H. Yan, "Regulating Cell Apoptosis on Layer-by-Layer Assembled Multilayers of Photosensitizer-Coupled Polypeptides and Gold Nanoparticles," *Scientific Reports*, vol. 6, no. 1, 2016.

[43] J. Y. Liao, D. Higgins, G. Lui, V. Chabot, X. C. Xiao, and Z. W. Chen, "Multifunctional TiO2–C/MnO2 core–double-shell nanowire arrays as high-performance 3D electrodes for lithium ion batteries," *Nano Letters*, vol. 13, no. 11, pp. 5467–5473, 2013.

[44] Z. G. Cheng, K. Cheng, and W. J. Weng, "SiO2/TiO2 nanocomposite films on polystyrene for light-induced cell detachment application," *ACS Applied Materials & Interfaces*, vol. 9, no. 3, pp. 2130–2137, 2017.

[45] F. Huang, A. T. Rad, W. Zheng, M. P. Nieh, and C. J. Cornelius, "Hybrid organic-inorganic 6FDA-6pFDA and multiblock 6FDA-DABA polyimide SiO2–TiO2 nanocomposites: synthesis, FFV, FTIR, swelling, stability, and X-ray scattering," *Polymer*, vol. 108, pp. 105–120, 2017.

[46] M. Momeni, H. Saghafian, F. Golestani-Fard, N. Barati, and A. Khanahmadi, "Effect of SiO2 addition on photocatalytic activity, water contact angle and mechanical stability of visible light activated TiO2 thin films applied on stainless steel by a sol gel method," *Applied Surface Science*, vol. 392, pp. 80–87, 2017.

[47] N. Saxena, T. Naik, and S. Paria, "Organization of SiO2and TiO2 nanoparticles into fractal patterns on glass surface for the generation of superhydrophilicity," *Journal of Physical Chemistry C*, vol. 121, no. 4, pp. 2428–2436, 2017.

[48] L. Shen, Y. F. Shen, and F. Li, "Corrigendum to 'Optimized utilization of NIR spectrum with interfacial $TiO_2/SiO_2/TiO_2$ trilayer in hybrid-integrated multijunction architecture' [Sol. Energy Mater. Sol. Cells 160 (2017) 425-429]," *Solar Energy Materials & Solar Cells*, vol. 161, pp. 460–460, 2017.

[49] L. Shen, Y. F. Shen, and F. Li, "Optimized utilization of NIR spectrum with interfacial $TiO_2/SiO_2/TiO_2$ trilayer in hybrid-integrated multijunction architecture," *Solar Energy Materials & Solar Cells*, vol. 160, pp. 425–429, 2017.

[50] W. Urbanski, K. Marycz, J. Krzak, C. Pezowicz, and S. F. Dragan, "Cytokine induction of sol-gel-derived TiO2 and SiO2 coatings on metallic substrates after implantation to rat femur," *International Journal of Nanomedicine*, vol. 12, pp. 1639–1645, 2017.

[51] Z. W. Yang, Y. Y. Shi, and B. Wang, "Photocatalytic activity of magnetically anatase TiO2 with high crystallinity and stability for dyes degradation: Insights into the dual roles of SiO2 interlayer between TiO2 and $CoFe2O_4$," *Applied Surface Science*, vol. 399, pp. 192–199, 2017.

[52] X. Chen and W. S. Kim, "Template-engaged solid-state synthesis of barium magnesium silicate Yolk@Shell particles and their high photoluminescence efficiency," *Chem-Eur J*, vol. 22, no. 21, pp. 7190–7197, 2016.

[53] X. C. Chen, J. Kim, T. Jung, J. Park, and W. S. Kim, "Architecture of directed-channel mesoporous silica/titania shell on bi-alkaline-earth carbonate particles for core-shell structure," *ChemistrySelect*, vol. 1, no. 13, pp. 3520–3526, 2016.

[54] X. C. Chen and W. S. Kim, "Template-engaged solid-state synthesis of barium-strontium silicate hexagonal tubes," *Journal of Alloys and Compounds*, vol. 647, pp. 1128–1135, 2015.

[55] X. Chen, T. Jung, J. Park, and W. S. Kim, "Preparation of single-phase three-component alkaline earth oxide of (BaSrMg)O: a high capacity and thermally stable chemisorbent for oxygen separation," *Journal of Materials Chemistry A*, vol. 3, no. 1, pp. 258–265, 2015.